IEEE Transactions on Industrial Electronics

“A Method for Computer-Aided Analysis of Differential Mode Input Filters”

Spasoje Miric,
Predrag Pejovic

IEEE TRANSACTIONS ON INDUSTRIAL ELECTRONICS, VOL. X, NO. Y, MONTH 2015 DOI: 10.1109/TIE.2017.2674584

A Method for Computer-Aided Analysis of Differential Mode Input Filters

Spasoje Mirić, *Student Member, IEEE,* and Predrag Pejović, *Senior Member, IEEE*

***Abstract*—A new method for computer-aided analysis of differential mode input filters is presented in the paper, aiming to compute in an efficient manner input current spectra of switching converters in a wide frequency range. The method is intended to facilitate computer-aided design of input filters, and it is based on simulation of accompanying averaged circuit and superimposing the switching ripple to the averaged waveforms. A method to derive a continuous-time averaged circuit model is described. To obtain the model, the converter is partitioned into a circuit part, characterized by equations common for describing electric circuits, and a modulator part, which generates duty ratio functions on the basis of voltages and currents of the circuit part of the converter. Five modulation methods are described, and superposition of associated switching ripple is formalized for each of them. The method is illustrated in simulation of three converters. Execution time is analyzed for three benchmark problems on several computers.**

***Index Terms*—Circuit simulation, computer aided analysis, continuous-time systems, electromagnetic interference, power conversion harmonics.**

I. Introduction

Although simulation of circuits with switches by digital computers emerged as a scientific topic as early as in 1956 [1], widely spread application of circuit simulation is usually associated with the emergence of SPICE [2]. In [2], many important concepts that influenced ideas about circuit simulation in the years to come have been established: the use of modified nodal analysis to describe the circuit, reduction of nonlinear circuit analysis to an iterative analysis of associated linear circuit in which nonlinear elements are linearized using the Taylor series expansions, application of implicit integration methods to solve differential equations arising from constitutive relations of reactive elements in transient analyses of dynamic circuits, the use of linear resistive equivalent circuits to represent reactive elements discretized applying the implicit numerical integration methods, automatic adjustment of the integration time step, a systematic language to describe the simulated circuit, to mention a few. The program offered several circuit analyses, which included DC analysis to obtain the quiescent operating point, AC analysis to compute the frequency response, and transient analysis to simulate dynamic response. The program evolved [3] by refining models and including new analysis types, leading to a comprehensive and mature simulation system [4]. It is worth to mention that SPICE is released under a permissive free software license, and became a basis to develop numerous proprietary software tools.

Although intended for simulation of integrated circuits, SPICE became a popular simulation tool in power electronics, [5]. Besides, ideas developed in SPICE significantly influenced the way of thinking about circuit simulation and affected even the tools not being direct descendants of SPICE. In power electronics, focus is in transient simulation of circuits that include switching elements. Such circuits have voltages and currents that expose rapid changes around the switching instants, resulting in wide spectra. Dynamics in power electronic circuits ranges from details of switching transitions, in order of tens of nanoseconds, over switching periods in the range of several microseconds, up to the control system transients that may last for tens and even hundreds of milliseconds. The problem gets even more complex when the converter is supplied through the mains, with the sinusoidal input voltage of the period in order of tens of milliseconds, resulting in even longer transients until the periodic steady state operation is reached. Such application of circuit simulators is in the focus of this paper [6]. Application of general purpose simulation tools to cover such a wide range of dynamic phenomena might be ineffective. Rapid variations in the simulated converter voltages and currents around switching instants require small time steps and results in a large number of steps, both in iteration over time and iteration over nonlinearity, yielding huge output files. Even worse, convergence problems are frequent, being caused by the initial point for iteration over nonlinearity not close enough to the solution, which is immanent around the switching instants, and might cause Newton-Raphson process to diverge. Furthermore, the component models are too detailed for some applications, and simulation parameters for such detailed simulations, like the values of parasitic capacitance and inductance, are frequently not known, resulting in low value of such detailed simulation results. Besides, if the spectrum of the converter input current is the simulation goal, in order to verify compliance with harmonic and electromagnetic interference standards [7], a relatively large number of equidistant samples of the input current for the converter operating in steady state is needed to compute the spectrum up to the desired frequency limit [8]. This requires a long simulation time to reach the steady state, and then requires additional effort to produce numerous regularly spaced samples of the input current to compute the spectrum.

Although general purpose simulation tools are frequently applied in power electronics [5], mentioned drawbacks initiated waves of intensive research aiming development of new

S. Mirić and P. Pejović are with the University of Belgrade, School of Electrical Engineering.

Manuscript received December 15, 2015; revised

simulation techniques that would suit the needs. A comprehensive review of such efforts is given in [9], summarizing several approaches to the problem. One approach is to simplify models of switching components, to use ideal switches and their generalized derivatives, piecewise linear models. Such approach is used in [10], [11], [12]. For example, as a heritage of [2], in [10] modified nodal analysis is used, as well as implicit integration methods. Application of components with discontinuous constitutive relations, or at least discontinuous derivatives, excluded the Newton-Raphson method to resolve problems related to nonlinear equations, and special algorithms had to be developed to resolve operating segments of piecewise linear element models [13]. As a result, a derivative of [12] seems to be frequently used in the power electronics community. Similar simulation concepts are applied in [14], which is used in power electronics research, development, and education.

A recent wave of interest in specialized simulation systems for power electronics and power systems is initiated by the hardware in the loop concept [15], [16], requiring the simulation result within specified time, but allowing simplified models of switching components.

A different approach in the analysis of switching power converters is based on averaging [9]. Early ideas that introduced averaging are given in [17], while a systematic and formalized method based on state-space model of the circuit under analysis is given in [18], [19], [20]. Motivation in developing these methods was to model converter sufficiently accurate to design a control loop. However, averaged circuit models are nonlinear, and to obtain transfer functions in order to apply linear system control theory, the resulting equation system should be linearized. To verify the control loop design, analysis and/or simulation of the nonlinear averaged circuit model might be of interest [21], [22]. Contrary to the switching circuits of power converters, nonlinearities in the averaged circuit model are mild and smooth, frequently in the form of a product of two continuous functions of time. It is possible that in some cases differential equations that model such systems are not stiff, and it might be computationally efficient to apply explicit numerical integration methods, which requires revisiting the topic of the integration method choice.

The method that will be proposed in this paper relies on [18], [19], [20], which formalized the averaging method on the basis of the converter state-space model in each of the switching combinations, and generalized the method to cover discontinuous conduction mode. Although the system of modified nodal equations used in [2] is very popular in circuit simulation due to easy formulation using the method of stamps, state-space model, a core of which is a system of the first order differential equations in normal form, offers interesting advantages in simulation of power converters, primarily in efficient solving of the resulting system of differential equations, as utilized in [23]. A drawback is in somewhat more complex methods required to obtain the state-space model on the basis of the circuit description. An approach to the problem of state-space averaging using symbolic computational tools is given in [24], automating the process.

To design differential mode input filter in order to suppress switching noise conducted to the mains [6], [25], [26], [27], spectrum of the converter input current is a required input. Furthermore, the spectrum should be available over a wide frequency range, which requires a huge number of evenly spaced data points of the input current steady state waveform during the line period [8]. High frequency components of the input current spectrum are essential, and the averaged input current waveform is not sufficient to obtain them. On the other hand, reaching the steady state may require simulation over many line periods, and an efficient simulation algorithm is needed. To meet these requirements, an initial idea of superimposing the switching ripple to the averaged circuit waveforms in order to obtain the input current waveform in an efficient manner is proposed in [28]. The idea is developed here, and the state-space averaged circuit model is used to resolve dynamics of the control circuit, which shapes the input current at low frequencies and modulates the high frequency components of the input current spectrum, effectively spreading the harmonics at multiples of the switching frequency. Out of these two phenomena, the state-space averaged circuit model covers the first, while for the high frequency spectrum the switching ripple has to be superimposed.

In order to be applied in proposed simulation algorithm, averaged circuit modeling is formalized in this paper. The converter under analysis is represented by an equivalent circuit for each of the switching combinations and characterized by state-space equations. This requires some prior knowledge about the circuit operation, which is expected to be available in a design process. The state-space models are averaged taking normalized durations of switching combinations, i.e. the duty ratio functions, as weighting coefficients. The duty ratio functions are treated as continuous functions of time, obtained as an output of the model of the modulator part of the converter. The output variables of the state-space model are chosen to include voltages across inductors for all of the switching combinations, to facilitate computation of the switching ripple, which is relevant both to construct actual current waveforms and to determine the operating mode. Furthermore, in the case current controlled modulation techniques are applied, the ripple determines the duty ratio functions. After specified outputs of the averaged state-space model are obtained, the switching ripple is simply computed and superimposed to the averaged inductor current waveforms. Next, waveforms of switch and diode currents are constructed, if required. In this manner, current spectra of inductors, switches, and diodes are obtained. To be utilize obtained waveforms in the design of differential mode input filters, propagation of the switching ripple through linear filtering circuits should be analyzed. In the proposed method, this task is performed in frequency domain, substituting the currents polluted with the switching ripple by corresponding current sources, according to the compensation theorem.

II. Continuous-Time Averaged Nonlinear Dynamic Model

The first step in obtaining of the converter waveforms is to form the converter state-space averaged model. The state-space averaging technique, originated in [18], is widely used in dynamic modeling of switching power converters, both in continuous [19] and in discontinuous [20] conduction modes. The method is based on decomposing the circuit under analysis into a sequence of k equivalent circuits that correspond to k specified switching combinations. For the three basic DC/DC switching converters, in the continuous conduction mode $k = 2$, while in the discontinuous conduction mode $k = 3$. For the time being, let us assume that the time intervals when each of the switching combinations is valid are known, and their durations are $d_i T_S$, where T_S is the switching period, $i \in \{1, \ldots k\}$, and d_i is normalized duration of the interval in which i^{th} switching combination is valid. The normalized durations, the duty ratios, should add up to 1,

$$\sum_{i=1}^{k} d_i = 1. \tag{1}$$

Usually, for d_1 a specific notation is used, the index being omitted, $d = d_1$.

For each of the switching combinations, the equivalent circuit is modeled by a set of ordinary differential equations of the first order in normal form over the circuit variables under derivatives, the state variables, packed into a vector of state variables $\vec{x}(t)$. These equations, the state equations, express derivatives of the state variables as functions of the state variables themselves, and the values of input variables, packed in a vector of input variables $\vec{u}(t)$, in the form

$$\frac{d\vec{x}(t)}{dt} = \vec{f}_i\left(\vec{x}(t), \vec{u}(t)\right). \tag{2}$$

This applies for each switching combination, $i \in \{1, \ldots k\}$.

On the other hand, relevant circuit variables, the output variables, packed into a vector of output variables $\vec{y}(t)$, are obtained through explicit algebraic expressions over the state variables and the input variables. These equations are the output equations, and they are purely algebraic, free of derivatives, in the form

$$\vec{y}(t) = \vec{g}_i\left(\vec{x}(t), \vec{u}(t)\right). \tag{3}$$

The state-space averaging technique aims to determine running averages of the state and the output variables over T_S, defined as

$$\langle z(t)\rangle = \frac{1}{T_S}\int_{t-T_S}^{t} z(\tau)\, d\tau. \tag{4}$$

Averaging is a linear operator. Assuming slow variation of $\vec{f}_i\left(\vec{x}(t), \vec{u}(t)\right)$ and $\vec{g}_i\left(\vec{x}(t), \vec{u}(t)\right)$, and constant values of d_i, averaged state equations are expressed in the form

$$\frac{d\langle\vec{x}(t)\rangle}{dt} = \sum_{i=1}^{k} d_i\ \langle\vec{f}_i\left(\vec{x}(t),\ \vec{u}(t)\right)\rangle \tag{5}$$

while averaged output equations are

$$\langle\vec{y}(t)\rangle = \sum_{i=1}^{k} d_i\ \langle\vec{g}_i\left(\vec{x}(t),\ \vec{u}(t)\right)\rangle. \tag{6}$$

In the case functions $\vec{f}_i\left(\vec{x}(t), \vec{u}(t)\right)$ and $\vec{g}_i\left(\vec{x}(t), \vec{u}(t)\right)$ are linear, or in the case of mild nonlinearity and/or slow variation of $\vec{x}(t)$ and $\vec{y}(t)$ with respect to T_S, the system of equations that constitute the averaged state-space model can be expressed as

$$\frac{d\langle\vec{x}(t)\rangle}{dt} = \sum_{i=1}^{k} d_i\ \vec{f}_i\left(\langle\vec{x}(t)\rangle,\ \langle\vec{u}(t)\rangle\right) \tag{7}$$

and

$$\langle\vec{y}(t)\rangle = \sum_{i=1}^{k} d_i\ \vec{g}_i\left(\langle\vec{x}(t)\rangle,\ \langle\vec{u}(t)\rangle\right). \tag{8}$$

Frequently, equivalent circuits that represent the converter under analysis in each of the switching combinations are linear, which results in common state-space averaged notation that involves averaged coefficient matrices [18], [19], [20].

The state-space averaging technique introduces a set of duty ratio variables, d_i, $i \in \{1, \ldots k\}$, in the averaged circuit model. All of the duty ratio variables are essentially discontinuous, and they have a fixed value that applies for a specified switching period. The values might change for the subsequent switching period, but within a switching period variation of the duty ratio variables cannot be assigned with a physical meaning. This causes the system to have properties that resemble continuous-time systems, and properties that resemble discrete-time systems. To simplify the analysis, and to treat all the variable parameters in a unified manner, the system would be treated as a continuous-time system in which the duty ratio variables are assumed as continuous functions of time.

In open loop systems, some of the duty ratio functions are the system input, and they can be treated as elements of the input vector, $\langle\vec{u}(t)\rangle$, along with voltages and currents of independent sources. In DC/DC converters, usually $d_1(t)$ corresponds to the switching combination in which the switch is on, and in open loop systems this duty ratio function is independent input variable, included in $\langle\vec{u}(t)\rangle$, while the other duty ratio functions are dependent on this one. For example, in the continuous conduction mode $d_2(t) = 1 - d_1(t)$. As mentioned, index of the first duty ratio function is usually omitted, and $d(t) = d_1(t)$ is used. In closed loop systems, all of the duty ratio functions are obtained as dependent on the circuit voltages and currents, which ultimately reduces to

$$d_i = d_i(t) = d_i\left(\langle\vec{x}(t)\rangle,\ \langle\vec{u}(t)\rangle\right) \tag{9}$$

for $i \in \{1, \ldots k\}$, general enough to cover for all situations. In this manner, the system of averaged state equations becomes

$$\begin{aligned}\frac{d\langle\vec{x}(t)\rangle}{dt} &= \sum_{i=1}^{k} d_i\left(\langle\vec{x}(t)\rangle,\ \langle\vec{u}(t)\rangle\right)\ \vec{f}_i\left(\langle\vec{x}(t)\rangle,\ \langle\vec{u}(t)\rangle\right)\\ &= \vec{F}\left(\langle\vec{x}(t)\rangle,\ \langle\vec{u}(t)\rangle\right)\end{aligned} \tag{10}$$

while the vector of output equations becomes

$$\begin{aligned}\langle\vec{y}(t)\rangle &= \sum_{i=1}^{k} d_i\left(\langle\vec{x}(t)\rangle,\ \langle\vec{u}(t)\rangle\right)\ \vec{g}_i\left(\langle\vec{x}(t)\rangle,\ \langle\vec{u}(t)\rangle\right)\\ &= \vec{G}\left(\langle\vec{x}(t)\rangle,\ \langle\vec{u}(t)\rangle\right).\end{aligned} \tag{11}$$

The duty ratio functions (9) are the ultimate control variables. Regardless of the control method used, its action results in changing the switching combination, which is represented by the duty ratio functions.

In some simulation methods, computation of $d_i(t)$ reduces to an algorithm that mimics the modulation circuit, resulting in the waveforms of signals that control switches. This approach is tedious, does not use advantages offered by the state-space averaging technique, and for modern digital control of switching power converters [29] it becomes extremely computationally demanding. Thus, in the approach proposed in this paper, $d(t)$ is obtained as a result of functional modeling of the modulator block, as it will be illustrated in examples. The result of such modeling is a duty ratio function which may be computed in any time point as a continuous function of time.

Solving the model that consists of (10) and (11) results in the vector of averaged state variables $\langle \vec{x}(t) \rangle$ and the vector of averaged output variables $\langle \vec{y}(t) \rangle$. To solve (10), appropriate numerical methods [30] are used.

At this point, it would be convenient to illustrate the technique on an example. A controlled buck converter, firstly analyzed in [31], and frequently reused as a benchmark circuit thereafter, like in [11], [13], is used as the example. The circuit is shown in Fig. 1, and specification of the parameters is given in Table I. To preserve space in the circuit diagram of Fig. 1, for the capacitor labeled C both the voltage and the current reference directions are indicated, while for the remaining capacitors only the current reference direction is indicated, assuming corresponding reference direction for the voltage as in the case of C. In order to simplify equations, for the initial analysis some of the parasitic effects would be neglected assuming $R_L = 0$, $R_C = 0$, $R_{ON} = 0$, and $R_1 >> R_{LOAD}$. The circuit contains five reactive elements, and in the case that algebraic degeneration does not occur it would be characterized by a system of state-space equations of the fifth order. In [31], the converter is partitioned into a power stage and the remaining part, which is the control circuit. Our partitioning separates "modulator, protection, and driver" part of the circuit, which on the basis of $v_F(t)$ and the switch current produces the pulse train that controls the switch, characterized by $d(t)$. Let us assume that at an interval of time the converter operates in the continuous conduction mode, with $i_L(t) > 0$, switching between two switching combinations: where the switch is on and the diode is off, and when the switch is off and the diode is on. In this case, the simplest one, the switching combination when the switch is on lasts for $d_1(t) = d(t)$, where according to the modulator specification [31] $d(t)$ is given by

$$d(t) = \begin{cases} 0, & v_F < 0 \\ \dfrac{v_F(t)}{10\,\mathrm{V}}, & 0 \le v_F(t) < 8.5\,\mathrm{V} \\ 0.85, & 8.5\,\mathrm{V} \le v_F(t). \end{cases} \tag{12}$$

This models the modulator in a functional way according to the continuous-time modeling requirements. In the continuous conduction mode, the state when the diode is on lasts for $d_2(t) = 1 - d(t)$.

According to the specified sequence of switching combinations the converter during a switching period passes through, and their durations, corresponding set of averaged state equations is

$$\frac{d\langle i_L(t)\rangle}{dt} = \frac{-\langle v_C(t)\rangle + d(t)\,\langle v_{IN}(t)\rangle}{L} \tag{13}$$

$$\frac{d\langle v_C(t)\rangle}{dt} = \frac{\langle i_L(t)\rangle}{C} - \frac{\langle v_C(t)\rangle}{C\,R_{LOAD}} \tag{14}$$

$$\frac{d\langle v_{CS}(t)\rangle}{dt} = \frac{\langle v_{CX}(t)\rangle}{R_X\,C_X} - \frac{R_X + R_S}{C_S\,R_S\,R_X}\,\langle v_{CS}(t)\rangle \tag{15}$$

$$\frac{d\langle v_{CX}(t)\rangle}{dt} = \frac{\langle v_{CS}(t)\rangle - \langle v_{CX}(t)\rangle}{R_X\,C_X} \tag{16}$$

$$\frac{d\langle v_{C0}(t)\rangle}{dt} = \frac{-\langle v_{C0}(t)\rangle + \langle v_{REF}(t)\rangle}{R_0\,C_0} \tag{17}$$

under mentioned simplifying assumptions introduced to avoid bulky equations. It is assumed $\langle v_{IN}(t)\rangle = V_{IN}$ and $\langle v_{REF}(t)\rangle = V_{REF}$. The output equations of the averaged model should necessarily include the output voltage, which in the simplified model reduces to a state variable

$$\langle v_{OUT}(t)\rangle = \langle v_C(t)\rangle \tag{18}$$

and $v_F(t)$, required by the modulator, which is a linear combination of two state variables

$$\langle v_F(t)\rangle = \langle v_{C0}(t)\rangle - \langle v_{CS}(t)\rangle. \tag{19}$$

The set of differential equations over state variables (13) to (17), accompanied by the set of output equations (18) and (19),

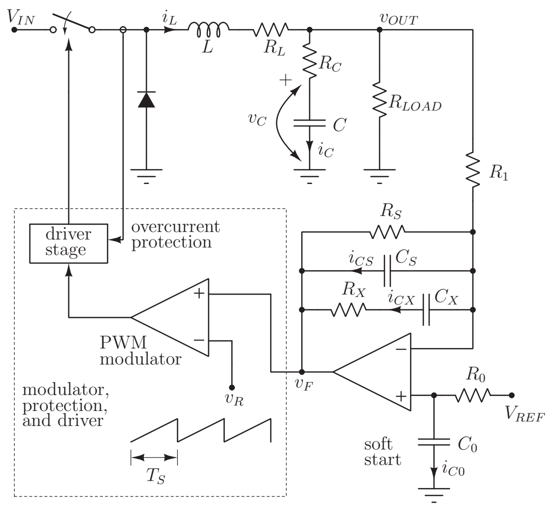

Fig. 1. Regulated buck converter.

TABLE I
PARAMETER SPECIFICATIONS FOR THE CIRCUIT OF FIG. 1

Power Stage	Control Circuit	PWM Modulator
$V_{IN} = 20\,\mathrm{V}$	$R_1 = 0.6\,\mathrm{k\Omega}$	$\alpha = 0.2\,\mathrm{V}/\mu\mathrm{s}$
$C = 1\,\mathrm{mF}$	$R_S = 300\,\mathrm{k\Omega}$	$d_{MAX} = 0.85$
$L = 200\,\mu\mathrm{H}$	$R_X = 4.7\,\mathrm{k\Omega}$	$I_{MAX} = 4\,\mathrm{A}$
$R_L = 0.25\,\Omega$	$C_S = 2\,\mu\mathrm{F}$	$f_S = 20\,\mathrm{kHz}$
$R_C = 0.1\Omega$	$C_X = 3.3\,\mu\mathrm{F}$	
$R_{ON} = 0.05\,\Omega$	$R_0\,C_0 = 1.8\,\mathrm{ms}$	
$R_{LOAD} = 5\,\Omega$	$V_{REF} = 5\,\mathrm{V}$	

and the averaged functional model of the modulator (12) constitute the continuous-time averaged nonlinear dynamic model. The model contains nonlinearities of the product type, which involve multiplication by $d(t)$, that are considered mild and should not yield convergence problems. The equations over state variables can be solved using an appropriate algorithm for solving systems of ordinary differential equations in normal form [30].

Developed continuous-time averaged nonlinear dynamic model of the converter of Fig. 1 applies solely for the continuous conduction mode, for $i_L(t) > 0$. Besides that, according to the circuit diagram and the specifications of Table I, the modulator also limits the switch current to $i_S(t) < 4\,\mathrm{A}$, which results in the same limit for $i_L(t)$, $i_L(t) < 4\,\mathrm{A}$. It should be noted that both of the constraints can be expressed in terms of instantaneous value of the inductor current, which is not provided by the continuous-time averaged nonlinear dynamic model. To account for this, ripple of the inductor current around the average value should be computed, to obtain the instantaneous value as a sum. Computation of the ripple is a topic of subsequent section, but at this point we should provide information about voltages across the inductor for each of the switching combinations as the output variables of the model, to facilitate computation of the ripple. When the switch is on, the voltage across the inductor in the simplified model ($R_L = 0$, $R_C = 0$, $R_{ON} = 0$) is

$$\langle v_1(t)\rangle = \langle v_{IN}(t)\rangle - \langle v_C(t)\rangle. \tag{20}$$

When the switch is off and the diode is on, the voltage across the inductor is

$$\langle v_2(t)\rangle = -\langle v_C(t)\rangle. \tag{21}$$

These two voltages should be appended to the vector of output variables, $\langle \vec{y}(t)\rangle$, to facilitate the ripple computation, which is also needed to determine limits of operation in the continuous conduction mode.

The converter under analysis exposes two additional operating modes: the discontinuous conduction mode, when intervals of $i_L(t) = 0$ occur, and the peak current limiting mode, when the switch is turned off as soon as its current reaches the specified limit. Handling of these modes requires information about the inductor current instantaneous value, which requires the inductor current ripple to be superimposed to the average value.

III. Superimposing Ripple

Superimposing ripple to the average value of the inductor current is initially proposed in [28] for the continuous conduction mode, and it is generalized here to cover the discontinuous conduction mode, the peak limiting current mode control, and the hysteresis window current mode control. In all of the cases, value of the voltage across the inductor is required for all of the switching combinations, and on the basis of these voltages and the durations of switching combinations waveform of the inductor current ripple is computed. It would be assumed that these voltages are included in the vector of output variables, and that they are available at the moment the inductor current ripple is computed.

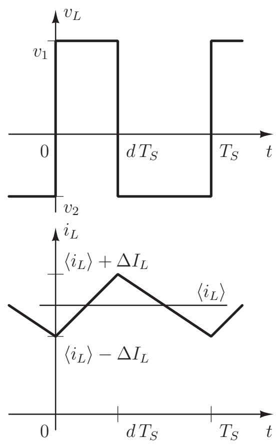

Fig. 2. Waveforms, continuous conduction mode.

A. Pulse Width Modulation in the Continuous Conduction Mode

This case is covered in [28], and it starts with the assumption that the switch is on during $d(t)\,T_S$, while the switch is off and the diode is on during the remaining part of the period

$$d_2(t) = d'(t) = 1 - d(t). \tag{22}$$

Waveform of the inductor current during this interval is given in Fig. 2. It is assumed that $0 \le d(t) \le 1$. Let us also assume that during the interval the switch is on the voltage across the inductor is $\langle v_1(t)\rangle$, while during the interval the diode is on the voltage across the inductor is $\langle v_2(t)\rangle$. Under the assumption of small variation of these voltages over a switching interval, the averaged state equation that governs the inductor current is

$$\langle v_L(t)\rangle = L\,\frac{\langle i_L(t)\rangle}{dt} = d(t)\,\langle v_1(t)\rangle + (1-d(t))\,\langle v_2(t)\rangle. \tag{23}$$

Peak-to-peak ripple of the inductor current during the interval the switch is on equals

$$2\,\Delta I_L(t) = \frac{\langle v_1(t)\rangle}{L}\,d(t)\,T_S \tag{24}$$

while during the interval the diode is on it is

$$-2\,\Delta I_L(t) = \frac{\langle v_2(t)\rangle}{L}\,(1-d(t))\,T_S. \tag{25}$$

To join the two values according to quasi steady state approximation [28], average of the values is used

$$\Delta I_L(t) = \frac{1}{4 f_S L}\left(d(t)\,\langle v_1(t)\rangle - (1-d(t))\,\langle v_2(t)\rangle\right). \tag{26}$$

After the ripple amplitude is determined by (26), waveform of the inductor current ripple is obtained as

$$\Delta i_L(t) = \begin{cases} \Delta I_L(t)\left(-1 + 2\,\dfrac{\tau}{d(t)\,T_S}\right), & \\ \qquad \text{for } 0 \le \tau < d(t)\,T_S & \\ \Delta I_L(t)\left(1 - 2\,\dfrac{\tau - d(t)\,T_S}{(1-d(t))\,T_S}\right), & \\ \qquad \text{for } d(t)\,T_S \le \tau < T_S & \end{cases} \tag{27}$$

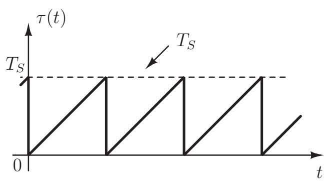

Fig. 3. Function $\tau(t)$, constant switching frequency.

where τ represents the running time variable within considered switching period, $\tau = t - t_0$, where t_0 corresponds to the beginning of the considered switching period, resulting in $0 \leq \tau < T_S$, as depicted in Fig. 3. Formal expression that defines τ is

$$\tau = t - T_S \lfloor \frac{t}{T_S} \rfloor \tag{28}$$

where $\lfloor \bullet \rfloor$ represents the floor function. Values of all variables are taken at the time point they correspond to, thus values of $\Delta I_L(t)$ and $d(t)$ may vary even within a switching period.

Finally, instantaneous value of the inductor current is obtained as a sum of the average value and the ripple

$$i_L(t) = \langle i_L(t) \rangle + \Delta i_L(t) \tag{29}$$

and this waveform is a basis to compute the switch current and the diode current, if their waveforms are required as the simulation output variables.

The value of $\Delta I_L(t)$ is also important as the continuous conduction mode boundary, and it should be computed even if the inductor current ripple is not of interest. The converter operates in the continuous conduction mode if $\Delta I_L(t) \leq \langle i_L(t) \rangle$, while otherwise the converter switches to the discontinuous conduction mode. In the discontinuous conduction mode, the sequence of states is different, as well as the methods to compute their durations.

The converter of Fig. 1 also includes the current limiting feature, as specified in Table I. The current limiting is activated when instantaneous value of the inductor current reaches the limit, which in terms of the introduced model limits the pulse width modulated continuous conduction mode to

$$\langle i_L(t) \rangle + \Delta I_L(t) < I_{MAX}. \tag{30}$$

In the case (30) is violated, the converter starts to operate in the peak limiting current mode control.

B. Pulse Width Modulation in the Discontinuous Conduction Mode

Waveform of the inductor current when the converter operates in the discontinuous conduction mode is given in Fig. 4. Peak value of the inductor current is obtained as

$$I_m(t) = \frac{\langle v_1(t) \rangle}{L} \, d(t) \, T_S. \tag{31}$$

Duration of the time interval when the diode is conducting is determined applying the volt-second balance [32] as

$$d_2(t) = -\frac{\langle v_1(t) \rangle}{\langle v_2(t) \rangle} \, d(t) \tag{32}$$

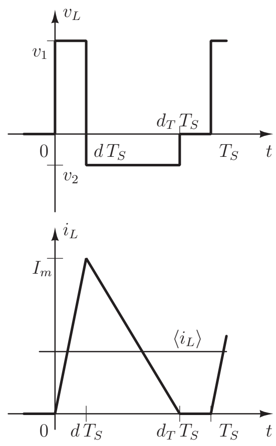

Fig. 4. Waveforms, discontinuous conduction mode.

while the duration of the time interval when neither the switch nor the diode conduct is given by

$$d_3(t) = 1 - d(t) - d_2(t) = 1 - \left(1 - \frac{\langle v_1(t) \rangle}{\langle v_2(t) \rangle}\right) d(t). \tag{33}$$

In the discontinuous conduction mode, average value of the inductor current is given by

$$\langle i_L(t) \rangle = \frac{1}{2} \left(d(t) + d_2(t) \right) I_m(t) \tag{34}$$

which expands to

$$\langle i_L(t) \rangle = \frac{\langle v_1(t) \rangle}{2 f_S L} \left(1 - \frac{\langle v_1(t) \rangle}{\langle v_2(t) \rangle}\right) d^2(t). \tag{35}$$

This is an algebraic equation which replaces corresponding differential equation (23); thus, the converter circuit suffers algebraic degeneration [32]. In the example of Fig. 1, (13) should be replaced by

$$\langle i_L(t) \rangle = \frac{\langle v_{IN}(t) \rangle - \langle v_C(t) \rangle}{2 f_S L} \, \frac{\langle v_{IN}(t) \rangle}{\langle v_C(t) \rangle} \, d^2(t) \tag{36}$$

in this mode, assuming the introduced simplifying set of parameter values.

To simplify the notation, let us define normalized duration of the time interval when $i_L(t) > 0$ as

$$d_T(t) = d(t) + d_2(t) = \left(1 - \frac{\langle v_1(t) \rangle}{\langle v_2(t) \rangle}\right) d(t) \tag{37}$$

In the case of the discontinuous conduction mode, waveform of the inductor current can be constructed directly as

$$i_L(t) = \begin{cases} I_m(t) \, \dfrac{\tau}{d(t)\, T_S}, & \text{for } 0 \leq \tau < d(t)\, T_S \\ I_m(t) \left(1 - \dfrac{\tau - d(t)\, T_S}{d_2(t)\, T_S}\right), & \text{for } d(t)\, T_S \leq \tau < d_T(t)\, T_S \\ 0, & \text{for } d_T(t)\, T_S \leq \tau < T_S \end{cases} \tag{38}$$

where τ is the offset time variable introduced in the same manner as for (27).

The discontinuous conduction mode is limited by the condition that the inductor is being discharged during a switching period, and it applies for $d_T(t) < 1$. If this condition is not met, the converter switches to the continuous conduction mode.

C. Peak Limiting Current Mode Control in the Discontinuous Conduction Mode

Treatment of this mode is essentially the same as for the pulse width modulated discontinuous conduction mode, except for the fact that the control variable is $I_m(t)$ instead of $d(t)$. In this case, the duty ratio that effectively controls the converter is computed as

$$d(t) = \frac{f_S L I_m(t)}{\langle v_1(t) \rangle}. \tag{39}$$

Computed value of $d(t)$ subsequently determines $d_2(t)$ and $d_3(t)$ according to (32) and (33), as well as $d_T(t)$ (37).

Average value of the inductor current is given by an algebraic equation, again

$$\langle i_L(t) \rangle = \frac{f_S L}{2} \left(\frac{1}{\langle v_1(t) \rangle} - \frac{1}{\langle v_2(t) \rangle} \right) I_m^2(t) \tag{40}$$

and the degeneration occurs. Waveform of the inductor current is generated applying (38).

Like in the pulse width modulated discontinuous conduction mode, this mode occurs for $d_T(t) < 1$. If this condition is violated, the converter operating mode switches to the peak limiting current mode controlled continuous conduction mode.

D. Peak Limiting Current Mode Control in the Continuous Conduction Mode

In this mode, the control variable is the maximum of the inductor current, $I_m(t)$, and the duty ratio $d(t)$ that effectively controls the converter is implicitly specified. Waveform of the inductor current is the same as for the pulse width modulated continuous conduction mode, given in Fig. 2. Amplitude of the current ripple is given by (26), accordingly. Maximum of the inductor current is obtained as

$$I_m(t) = \langle i_L(t) \rangle + \Delta I_L(t) \tag{41}$$

which results in the duty ratio of

$$d(t) = \frac{\langle v_2(t) \rangle + 4 f_S L \left(I_m(t) - \langle i_L(t) \rangle \right)}{\langle v_1(t) \rangle + \langle v_2(t) \rangle}. \tag{42}$$

this value applies if the computed value satisfies $d(t) < 1$. Otherwise, the value $d(t) = 1$ is used.

Boundary between this mode and the discontinuous conduction mode is as defined for the pulse width modulated case, expressed in terms of $I_m(t)$ as $I_m(t) - 2\,\Delta I_L(t) > 0$. If the condition is violated, the converter operation switches to the discontinuous conduction mode.

Construction of the inductor current waveform is the same as for the continuous conduction mode, as specified by (27) and (29).

It should be underlined that the model applies for period-1 operation only, $0 \le d(t) < \frac{1}{2}$ [32]. The result could be generalized for period-1 operation beyond this limit in the case an artificial ramp is introduced in the modulator [32]. Effects of higher order periodicity and aperiodic response on the averaged model are significant, as analyzed in [33], [34].

E. Hysteresis Window Current Mode Control

This control method implicitly provides $\langle i_L(t) \rangle$ and $\Delta I_L(t)$ by specifying

$$i_{L\,max}(t) = \langle i_L(t) \rangle + \Delta I_L(t) \tag{43}$$

and

$$i_{L\,min}(t) = \langle i_L(t) \rangle - \Delta I_L(t). \tag{44}$$

Algebraic degeneration occurs since $\langle i_L(t) \rangle$ is implicitly specified by an algebraic equation, which removes the differential equation over $\langle i_L(t) \rangle$ (13) and replaces it with

$$\langle i_L(t) \rangle = \frac{i_{L\,min} + i_{L\,max}}{2}. \tag{45}$$

Interval when the inductor is exposed to $\langle v_1(t) \rangle$ is $d(t)\,T_S(t)$, specified by

$$2\,\Delta I_L(t) = \frac{\langle v_1(t) \rangle}{L}\, d(t)\, T_S(t) \tag{46}$$

while the interval when the inductor is exposed to $\langle v_2(t) \rangle$ is $d_2(t)\,T_S(t)$, specified by

$$-2\,\Delta I_L(t) = \frac{\langle v_2(t) \rangle}{L}\, d_2(t)\, T_S(t). \tag{47}$$

Solving (46) and (47) over time intervals yields

$$d(t)\,T_S(t) = \frac{2\,L\,\Delta I_L(t)}{\langle v_1(t) \rangle} \tag{48}$$

and

$$d_2(t)\,T_S(t) = -\frac{2\,L\,\Delta I_L(t)}{\langle v_2(t) \rangle} \tag{49}$$

which results in the switching period of

$$T_S(t) = 2\,L\,\Delta I_L(t) \left(\frac{1}{\langle v_1(t) \rangle} - \frac{1}{\langle v_2(t) \rangle} \right) \tag{50}$$

which in this case is a function of time, not a constant parameter as in the four operating modes described previously. This slightly affects the process (28) of determining τ, needed to superimpose the ripple, since the upper limit for τ is variable now, as shown in Fig. 5. Also, the variable switching period results in variable switching frequency

$$f_S(t) = \frac{1}{T_S(t)}. \tag{51}$$

From (48) and (50) the duty ratio that effectively controls the converter and enters the continuous-time averaged nonlinear model is obtained as

$$d(t) = \frac{\langle v_2(t) \rangle}{\langle v_2(t) \rangle - \langle v_1(t) \rangle}. \tag{52}$$

Obtained value should satisfy $0 \le d(t) \le 1$. In the case the condition is violated, the converter exits current programmed mode and enters pulse width controlled mode either for $d(t) = 0$ or $d(t) = 1$, exiting the algebraic degeneration.

Another boundary phenomenon occurs in the case the method is applied in a converter with diode, that might enter

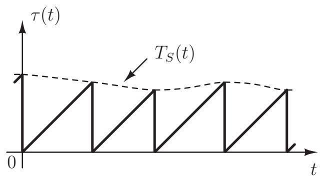

Fig. 5. Function $\tau(t)$, variable switching frequency.

discontinuous conduction mode. In the case $i_{L\,min} < 0$ the converter locks into the discontinuous conduction interval, with $\langle i_L(t)\rangle = 0$, until the controller assigns the minimum inductor current value greater than zero.

F. Constructing Waveforms of Currents for Switches and Diodes

In some applications, actual waveforms for currents of switches and diodes are needed, not just their averaged values. These waveforms could be constructed after the waveform of corresponding inductor current is constructed, since the conducting intervals are known. The switch current is given by

$$i_S(t) = \begin{cases} i_L(t), & 0 \le \tau < d(t)\,T_S \\ 0, & \text{otherwise} \end{cases} \tag{53}$$

while the diode current is given by

$$i_D(t) = \begin{cases} 0, & 0 \le \tau < d(t)\,T_S \\ i_L(t), & \text{otherwise} \end{cases} \tag{54}$$

which covers both for the continuous conduction mode and the discontinuous conduction mode.

IV. Application Examples

In order to illustrate functionality of the proposed simulation method, three systems are analyzed. The examples are selected to demonstrate application of various control methods and to show how the method can be applied in the design of differential mode input filters. Two of the examples involve frequently used benchmark circuits [31], while the third one represents a common differential mode filter design problem.

In each of the examples, in the first stage averaged waveforms are constructed. The term “waveforms” is used to represent voltages, currents, and duty ratio functions that determine duration for each switching combination, like $d(t)$. All the waveforms are treated in the same way, as continuous functions of time.

To generate the continuous-time averaged nonlinear dynamic model, state equations for each of the switching combinations are generated using symbolic computation. Similar approach is used in [24], but in our application we used Maxima [35]. On the basis of values of the state variables and the input vector variables, the duty ratio functions are formed (9). This step might involve computation of the ripple amplitude, and is performed by a control block which models the modulator. Finally, the continuous-time averaged nonlinear dynamic model is formed as (10) and (11). Obtained system of differential equations (10) is smooth, and can be solved applying a suitable numerical method [30].

After the continuous-time nonlinear dynamic model is solved and all the waveforms relevant for computation of the ripple are obtained, the ripple is computed applying methods of Section III and superimposed to the obtained waveforms of averaged inductor currents. On the basis of the inductor currents, the waveforms of corresponding switches and diodes are computed.

Each of the described simulation examples is implemented in two programming languages, Python [36], [37], accompanied with appropriate libraries [38], [39], [40], and Julia [41], [42], since an auxiliary task was to test efficiency of a relatively new programming language Julia and its feature of being a compiled language.

A. Regulated Buck Converter

As a first example, simulation of a frequently used benchmark circuit [31] is performed. Although not immediately related to the differential mode filter design, the circuit is a suitable example, since in the startup transient it passes through three operating modes: the pulse width modulated continuous conduction mode, the peak limiting current controlled mode, and the pulse width modulated discontinuous conduction mode. These are three methods out of five analyzed in Section III. The circuit is already used as an example in illustrating derivation of the continuous-time averaged nonlinear model in Section II, with a set of simplifying assumptions introduced. Here, the circuit simulation is performed without the simplifying assumptions, with the parameter values as specified in [31] and reproduced in Table I.

The simulation task of the first example is the same as in [31], to simulate the startup transient. Initial values for all of the state variables are set to zero, and the converter is simulated for the first 20 ms of operation.

Simulation result for the inductor current is presented in Fig. 6, where the thick curve represents the averaged waveform of the inductor current, obtained as a solution of the continuous-time nonlinear dynamic model, while the thin gray line represents the instantaneous value of the inductor current, obtained superimposing the ripple to the average current waveform. The diagram matches the result of [31]. In the time interval of about $0 \le t < 0.7\,\text{ms}$, the converter operates in the pulse width modulated continuous conduction mode. As the average value of the inductor current rises, the inductor current approaches the current limit, and the converter enters the peak limiting current controlled mode in the time interval of about $0.7\,\text{ms} \le t < 2\,\text{ms}$. Next, the control circuit reduces the duty ratio and the inductor current average value drops down, resulting in the converter operating in the discontinuous conduction mode in the time interval approximately $2.7\,\text{ms} \le t < 4.2\,\text{ms}$. After this interval, until the end of the transient, the converter operates in the pulse width modulated continuous conduction mode, while ringing of the inductor current average value is being damped.

B. Switch-Mode Rectifier

As a second example, a rectifier with input current shaping is taken. The example is closely related to the topic of this

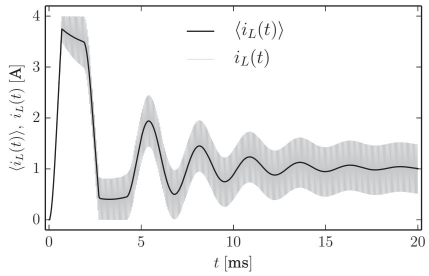

Fig. 6. Regulated buck converter, inductor current.

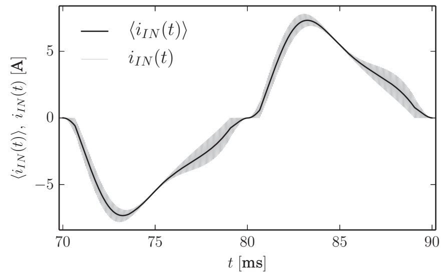

Fig. 8. Input current.

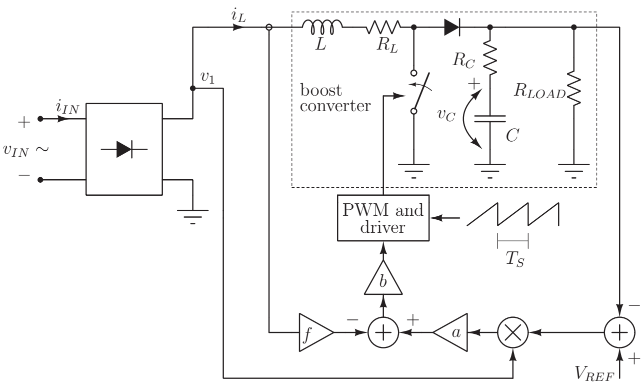

Fig. 7. Rectifier with input current shaping.

paper, and the design of the input filter intended to reduce the spectral part of the input current in high frequency range is discussed. Circuit and control diagram of the converter are shown in Fig. 7. The converter is used as an example in [31], again, and the results presented there would serve as a reference for comparison.

In the circuit of Fig. 7, when filter of the output voltage ripple discussed in the second part of the example in [31] is removed, there are only two state variables, the inductor current and the capacitor voltage, $\vec{x}(t) = [i_L(t), v_C(t)]^T$, since all three of the control gains a, b, and f are frequency independent. Parameters of the system are summarized in the Table II.

Aim of the simulation example is to illustrate application of the method in the design of input filters [25], [26]. The first step in designing the input filter is to understand the filtering requirements, which reduces to obtaining the spectrum of the converter steady state input current in the frequency range of interest. To obtain the spectrum, the input current waveform should be available over one period in a sufficient number of evenly spaced points to cover the frequency range of interest [8]. If the highest frequency of interest in the spectrum of the input current is f_{max}, than the time step between two successive data points is

$$\Delta t = \frac{1}{2\,f_{max}}. \tag{55}$$

On the other hand, the frequency resolution of the result is dependent on the time span of the frame covered by the simulation, $T_0 = 1/f_0$, which usually corresponds to one period of the line voltage,

$$\Delta f = \frac{1}{T_0}. \tag{56}$$

This results in

$$N_P = \frac{T_0}{\Delta t} = 2\,\frac{f_{max}}{f_0} \tag{57}$$

data points, and it is possible that this is a huge number, requiring an efficient algorithm to handle.

In the example of Fig. 7, to reach the steady state the converter is simulated starting from the zero initial conditions for all of the state variables over 100 ms, which corresponds to five periods of the line voltage. Analyzing the diagrams, a conclusion is made that after 70 ms the converter may be considered as operating in steady state. At this stage, constructing of actual waveforms by superimposing ripple is not required, it is sufficient to analyze the diagrams of averaged waveforms. After the steady state is reached, waveforms of relevant currents are constructed, and in the time interval from 70 ms to 90 ms waveform of the input current is presented in Fig. 8.

After the waveform of the input current is obtained, its compliance with standards [7] is analyzed in frequency domain, assuming that the line impedance, as well as the input filter to be introduced, do not affect the inductor current significantly. This assumption is justified by the fact that the differential mode switching noise introduced in the power line is negligible in comparison to the line voltage. Thus, the analysis of the switching ripple propagation is reduced to an analysis of a linear circuit in frequency domain, in which the current polluted by the switching ripple is replaced by a corresponding current source. In this manner, in Fig. 9 the converter is represented by a current source having the waveform obtained as the simulation result, i_{IN}. According

TABLE II
SIMULATION PARAMETERS FOR THE SWITCH-MODE RECTIFIER

Power Stage	Control Circuit
$V_{IN} = 300\,\mathrm{V}$	$f_S = 100\,\mathrm{kHz}$
$C = 0.5\,\mathrm{mF}$	$\alpha = 0.2\,\mathrm{V}/\mu\mathrm{s}$
$L = 0.4\,\mathrm{mH}$	$d_{MAX} = 0.85$
$R_L = 1\,\Omega$	$V_{REF} = 320\,\mathrm{V}$
$R_C = 0.1\Omega$	$a = 2\times10^{-4}\,\mathrm{V}^{-1}$
$R_{ON} = 0.1\,\Omega$	$f = 0.2\,\mathrm{V/A}$
$R_{LOAD} = 100\,\Omega$	$b = 30$

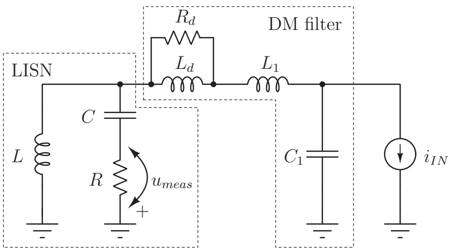

Fig. 9. LISN, the input filter, and the current source that represents the converter. LISN parameters: $R = 50\,\Omega$, $L = 50\,\mu$H, $C = 250\,$nF.

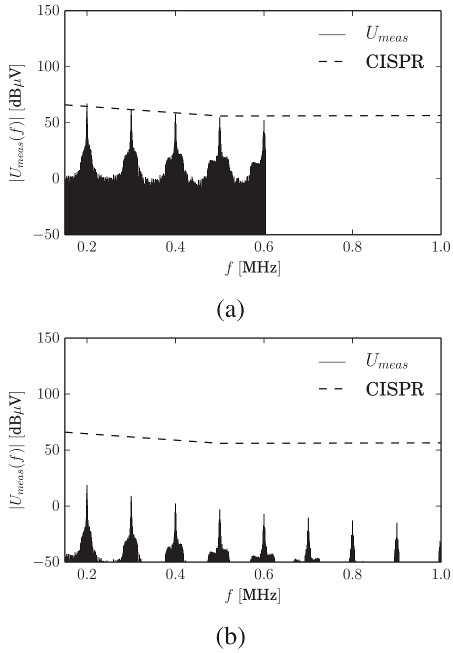

Fig. 10. Boost converter, noise voltage: (a) without input filter; (b) with input filter. Filter parameters: $C_1 = 5\ \mu$F, $L_1 = 1.266\ \mu$H, $L_d = 12.66\ \mu$H, $R_d = 0.6371\ \Omega$.

to applicable standards, to stabilize the line impedance and to measure the introduced differential mode switching noise, a line impedance stabilization network [7] is used, labeled as LISN in Fig. 9, where the test points to measure the differential mode noise voltage are labeled as u_{meas}.

After the circuit is transformed to the equivalent circuit of Fig. 9 applying the compensation theorem, the analysis is performed in the frequency domain. In Fig. 10 (a) the results are presented in the case the differential mode filter, labeled as “DM filter” in Fig. 9 omitted, indicating that the noise is slightly above the limit specified by the standard [7]. After the differential mode input filter [25] is introduced, the resulting noise voltage spectra are shown in Fig. 10 (b), indicating complete compliance with the standard.

It should be noted that this stage, in the frequency domain analysis after application of the compensation theorem, the switching ripple is introduced in other circuit variables than the currents of inductors, switches and diodes.

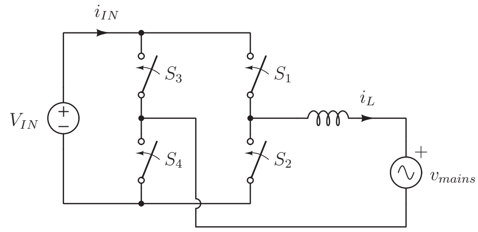

Fig. 11. Inverter system.

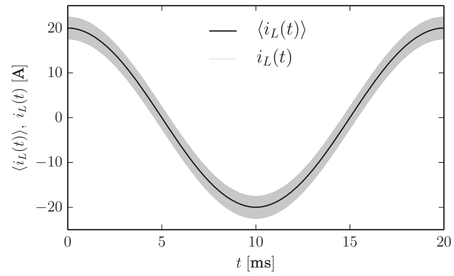

Fig. 12. Inverter, inductor current.

C. Inverter System with the Hysteresis Window Current Mode Control

In order to illustrate application of the method to systems with variable switching frequency, an inverter system intended to transfer the power provided by a voltage source V_{IN} to the mains, modeled by the voltage source v_{mains}, shown in Fig. 11, is analyzed. It is assumed that the system is supplied by a constant voltage source $V_{IN} = 450\,$V, and that the mains voltage is $v_{mains} = V_m \cos(\omega_0 t)$, where $V_m = 230\sqrt{2}\,$V, $\omega_0 = 2\pi \times 50\,$Hz. To couple the inverter and the mains an inductor of $L = 140\,\mu$H is used, and the inverter is operated switching from the state when S_1 and S_4 are on to the state when S_2 and S_3 are on, and vice versa, to provide the inductor current with the average value $\langle i_L \rangle = I_m \cos(\omega_0 t)$, $I_m = 20\,$A, with the peak-to-peak ripple of $2\,\Delta I_L = 5\,$A. The example is similar to the one used in [28], but instead of the constant frequency control, hysteresis window current mode control is used.

The system is simulated, and diagram of the inductor current is presented in Fig. 12. To verify compliance of the obtained inductor current with standards, the method of equivalent circuit of Fig. 9 is applied, and the resulting interference voltage spectrum is shown in Fig. 13 (a). The spectrum does not meet the requirements, and an one stage filter [25] shown in Fig. 9 is applied. Resulting spectrum of the noise voltage is given in Fig. 13 (b), and it complies with the requirements.

To illustrate construction of waveforms of switch and diode currents, let us consider the inverter of Fig. 11. Each of the switches in the inverter is built using a unidirectional controlled switch and an antiparallel diode, as depicted in Fig. 14. Thus, the current of the switch, i_{Sk}, consists of the controlled switch current, i_{SkS}, and the diode current, i_{SkD}, according to $i_{Sk} = i_{SkS} - i_{SkD}$. Based on the inductor current, determined as shown in Fig. 12, waveforms of $i_{S1S}(t)$ and $i_{D2S}(t)$ are constructed, as well as the input current waveform

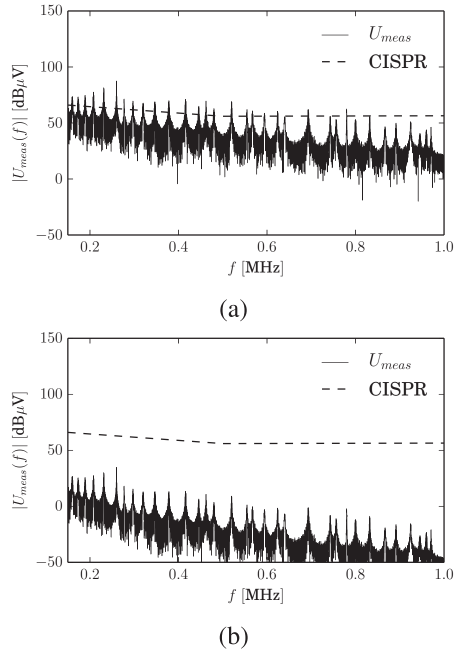

Fig. 13. Inverter system, noise voltage: (a) without filter; (b) with the filter. Input filter parameters: $C_1 = 5$ μF, $L_1 = 7.9889$ μH, $L_d = 79.889$ μH, $R_d = 1.6003$ Ω.

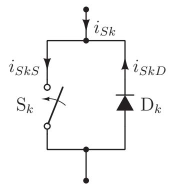

Fig. 14. The switch structure.

$i_{IN}(t)$, and they are in the time interval from 2.50 ms to 2.55 ms presented in Fig. 15. Obtained value of $I_{IN} = 7$ A meets the theoretical prediction based on the conservation of energy.

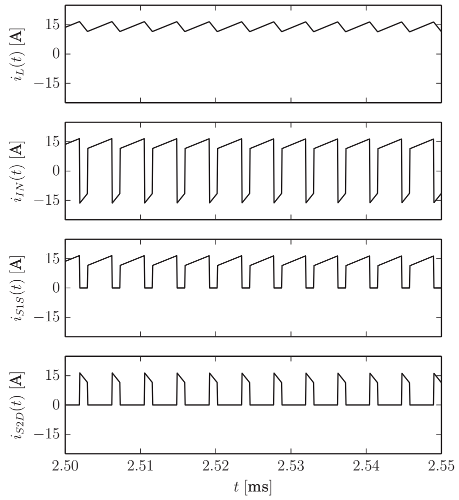

Fig. 15. Inverter system: $i_L(t)$, $i_{IN}(t)$, $i_{S1}(t)$, and $i_{D2}(t)$.

TABLE III
EXECUTION TIMES ANALYSIS.

	buck, 20 kpts		boost, 100 kpts		boost, 250 kpts	
	Python	Julia	Python	Julia	Python	Julia
computer #1						
min [s]	2.79	0.60	11.06	1.17	27.18	1.91
mean [s]	2.89	0.61	11.32	1.20	28.07	1.96
max [s]	3.00	0.63	12.17	1.23	29.47	2.01
st. dev. [s]	0.06	0.01	0.28	0.02	0.71	0.03
computer #2						
min [s]	6.72	1.91	25.98	2.89	64.19	4.06
mean [s]	6.93	1.93	26.79	2.92	66.70	4.10
max [s]	7.61	1.95	28.46	2.96	72.92	4.21
st. dev. [s]	0.24	0.01	0.71	0.02	2.14	0.04
computer #3						
min [s]	8.71	2.07	33.31	3.72	83.81	5.20
mean [s]	8.83	2.30	34.05	3.86	85.48	5.24
max [s]	8.96	2.64	35.59	4.05	88.04	5.29
st. dev. [s]	0.07	0.16	0.71	0.10	1.23	0.03
computer #4						
min [s]	8.78	1.47	33.36	2.92	94.55	5.24
mean [s]	9.81	1.67	39.78	3.18	99.97	6.07
max [s]	10.89	1.82	41.82	3.59	105.00	6.28
st. dev. [s]	0.90	0.14	1.88	0.24	3.11	0.29
computer #5						
min [s]	37.66	8.82	142.19	13.48	355.32	20.14
mean [s]	38.24	8.90	144.28	14.19	359.06	21.20
max [s]	39.48	9.09	145.80	14.43	363.99	21.56
st. dev. [s]	0.39	0.06	0.97	0.21	2.46	0.35

D. Comparison of Simulation Times

Although simulation time is not an exact parameter that characterizes the algorithm, it is the essential information for application of simulation methods. The simulation time depends on the computer which performs the simulation, as well as the tasks being performed by the computer in parallel. Thus, the same simulation task performed on the same computer produces a different simulation time result for each run. To analyze efficiency of the proposed algorithm, three simulation tasks are performed on five computers, and each simulation is repeated twenty times to obtain minimum, maximum, and mean execution time, as well as standard deviation of the obtained results. During the simulations, the computers were released of other user initiated tasks that would run in parallel. The simulation tasks covered previously described examples: simulation of the buck converter in 20×10^3 data points (20 kpts), simulation of the boost converter in 100×10^3 data points (100 kpts), and simulation of the boost converter in in 250×10^3 data points (250 kpts). The first computer is equipped with Intel(R) Core(TM) i5-4690 CPU at 3.50 GHz $\times$ 4, with 7.7 GiB of memory under 64-bit Ubuntu 14.04 LTS operating system, the second is Intel(R) Pentium(R) 3556U at 1.70 GHz $\times$ 2, with 3.8 GiB of memory, under 64-bit Ubuntu 15.10 operating system, the third is Intel(R) Core(TM) 2 Duo CPU T7700 at 2.40 GHz $\times$ 2, with 3008 MiB of memory, under 64-bit Ubuntu MATE 15.10 operating system, the fourth is Intel(R) Core(TM) 2 Quad CPU Q9300 at 2.50 GHz $\times$ 4, with 3.9 GiB of memory, under 64-bit Ubuntu 14.04 LTS operating system, while the fifth is a computer is of the netbook type, not intended for intensive numerical computations, having Intel(R) Atom(TM) CPU N450 at 1.66 GHz $\times$ 2, with 991.4 MiB of memory, under 32-bit Ubuntu 14.04 LTS operating system. The computer data are reproduced as reported by the operating system.

The results for the execution time are summarized in Table III, and they indicate that even for the most complex of the simulation tasks the simulation time remained moderate, regardless of the computer being used, including even a netbook computer not intended for intensive computations. The algorithms implemented in Julia required about an order of magnitude lower time to execute, which is a fact that deserves attention for complex simulation tasks.

V. Conclusions

In this paper, a method for simulation of switching power converters is proposed. The method is primarily intended for application in the design of differential mode input filters, where the problem requires computation of steady state input current spectra in a wide frequency range. Reaching the steady state requires long simulation of a startup transient, and computing wide spectra requires a huge number of evenly spaced samples per a steady state period, thus an efficient algorithm is needed to fulfill the requirements.

Proposed algorithm is based on simulation of the state-space averaged circuit and superimposing ripple to the obtained averaged waveforms. At first, the converter continuous-time averaged nonlinear dynamic model is developed on the basis of the state-space averaging technique. The model is treated as continuous in time, generalizing the duty ratio functions as continuous. Formulation of the model is formalized, and it is shown that it may contain smooth nonlinearities. The model provides a set of the first order differential equations in normal form, possibly nonlinear, which is solved applying appropriate numerical algorithms for initial value problems.

To form the model, the converter under analysis is partitioned into a circuit part and a modulator part. The circuit part contains all the elements convenient to model by applying electric circuit theory, while the modulator part is described functionally as it generates the duty ratio functions on the basis of averaged state variables and output variables. This partitioning is convenient to model a wide range of controller circuits, starting from the pulse width modulator as the simplest, up to the complex control algorithms implemented in digital signal processor platforms. The common point for the whole range of systems is that their output is information about normalized duration in which a certain switching combination is valid, enabling a corresponding sets of state equations to be averaged. The duty ratio functions are treated as continuous functions of time, being weighting functions for the state-space averaging process. Several modulator structures are considered and illustrated in examples, starting from the common pulse width modulator in the continuous conduction mode, the pulse width modulator in the discontinuous conduction mode, the modulators that implement the peak limiting current mode control both in the discontinuous conduction mode and the continuous conduction mode, and finally the modulator that implements hysteresis window current mode control with variable switching frequency. To implement the current control modulation algorithms, as well as to distinguish the conduction mode either as continuous or discontinuous, information about the inductor current ripple is required. In order to provide that information, voltage across the inductor should be provided for each of the switching combinations as an output variable of the model.

After the averaged waveforms of the circuit variables are computed, the ripple is superimposed to relevant currents. In the algorithm described in this paper, this applies to inductor currents, as well as to construction of switch and diode currents. Algorithms to superimpose the ripple are derived for all five modulation methods considered in the paper. Averaged circuit currents, voltages, duty ratio functions, and ripple amplitudes are treated as continuous functions of time. Formulae to compute the ripple are provided.

Application of the proposed algorithm is illustrated in three examples. The first of them illustrates application of the method in a benchmark circuit of a controlled buck converter. The example illustrates the converter operation with pulse width modulation both in the continuous and the discontinuous conduction mode, as well as the operation in the peak limiting current mode control in the continuous conduction mode. The second of the examples covers a rectifier with a boost converter utilized to shape the input current. The input current waveform is obtained applying proposed techniques of averaged circuit simulation and ripple superposition, and its spectrum is computed. To analyze compliance with standards, propagation of the switching ripple is analyzed in frequency domain, applying the compensation theorem to represent the converter input current with superimposed ripple by a current source. This source is utilized as a load to the line impedance stabilization network. It is shown that the resulting noise voltage spectrum is slightly above the limits imposed by applicable standards, and appropriate filter is designed to resolve the problem. The frequency domain analysis is performed again, and it is shown that the designed filter suffices. The third problem considers application of the hysteresis window current mode control in an inverter system that transfers power from a DC source to the mains. The mains current is obtained, and the noise voltage spectrum is computed in frequency domain, applying the compensation theorem. It is shown that the waveform does not meet the requirements, and appropriate differential mode filter is designed to reduce the interference. The analysis is performed again, and the resulting noise spectrum is shown to meet the requirements.

To illustrate efficiency of the algorithm, the simulation time data are provided for three simulation tasks on five computers. On each of the computers, each simulation is performed twenty times to obtain the data for statistical analysis. The data indicate that the method is fast, and that the algorithm implemented in Julia language completed in an order of magnitude lower time than the algorithm implemented in Python. In both cases, the simulation time was moderate and encouraged application of the proposed method.

References

[1] S. Denison and D. Taylor, “The use of digital computers in obtaining solutions to electric-circuit problems involving switching operations,”

Proceedings of the IEE-Part B: Radio and Electronic Engineering, vol. 103, no. 1S, pp. 35–46, 1956.

[2] L. W. Nagel, “Spice2: A computer program to simulate semiconductor circuits,” *ERL Memo ERL-M520*, 1975.

[3] ——, “The life of spice,” in *1996 Bipolar Circuits and Technology Meeting*, 1996.

[4] A. Vladimirescu, *The SPICE book*. John Wiley & Sons, Inc., 1994.

[5] M. H. Rashid, *Spice for power electronics and electric power*. CRC Press, 2012.

[6] J. Mahdavi, M. Tabandeh, and A. Shahriari, “Comparison of conducted rfi emission from different unity power factor ac/dc converters,” in *Power Electronics Specialists Conference, 1996. PESC’96 Record., 27th Annual IEEE*, vol. 2. IEEE, 1996, pp. 1979–1985.

[7] C. R. Paul, *Introduction to electromagnetic compatibility*. John Wiley & Sons, 2006, vol. 184.

[8] S. K. Mitra and Y. Kuo, *Digital signal processing: a computer-based approach*. McGraw-Hill New York, 2006, vol. 2.

[9] D. Maksimović, A. M. Stanković, V. J. Thottuvelil, and G. C. Verghese, “Modeling and simulation of power electronic converters,” *Proceedings of the IEEE*, vol. 89, no. 6, pp. 898–912, 2001.

[10] P. Pejović and D. Maksimović, “Pets-a simulation tool for power electronics,” in *Computers in Power Electronics, 1996., IEEE Workshop on*. IEEE, 1996, pp. 1–8.

[11] D. Li, R. Tymerski, and T. Ninomiya, “Pecs-an efficient solution for simulating switched networks with nonlinear elements,” *Industrial Electronics, IEEE Transactions on*, vol. 48, no. 2, pp. 367–376, 2001.

[12] J. Alimeling and W. P. Hammer, “Plecs-piece-wise linear electrical circuit simulation for simulink,” in *Power Electronics and Drive Systems, 1999. PEDS’99. Proceedings of the IEEE 1999 International Conference on*, vol. 1. IEEE, 1999, pp. 355–360.

[13] P. Pejović and D. Maksimović, “An algorithm for solving piecewise-linear networks that include elements with discontinuous characteristics,” *Circuits and Systems I: Fundamental Theory and Applications, IEEE Transactions on*, vol. 43, no. 6, pp. 453–460, 1996.

[14] U. Drofenik, J. Kolar *et al.*, “New circuit simulation applets for online education in power electronics,” in *e-Learning in Industrial Electronics (ICELIE), 2011 5th IEEE International Conference on*. IEEE, 2011, pp. 70–75.

[15] M. Matar and R. Iravani, “Fpga implementation of the power electronic converter model for real-time simulation of electromagnetic transients,” *Power Delivery, IEEE Transactions on*, vol. 25, no. 2, pp. 852–860, 2010.

[16] D. Majstorović, I. Čelanović, N. D. Teslić, N. Čelanović, and V. Katić, “Ultralow-latency hardware-in-the-loop platform for rapid validation of power electronics designs,” *Industrial Electronics, IEEE Transactions on*, vol. 58, no. 10, pp. 4708–4716, 2011.

[17] G. W. Wester, “Low-frequency characterization of switched dc-dc converters,” Ph.D. dissertation, California Institute of Technology, 1972.

[18] S. Ćuk, “Modelling, analysis, and design of switching converters,” Ph.D. dissertation, California Institute of Technology, 1977.

[19] R. Middlebrook and S. Ćuk, “A general unified approach to modelling switching-converter power stages,” in *Power Electronics Specialists Conference, 1976 IEEE*. IEEE, 1976, pp. 18–34.

[20] S. Ćuk and R. Middlebrook, “A general unified approach to modelling switching dc-to-dc converters in discontinuous conduction mode,” in *Power Electronics Specialists Conference, 1977 IEEE*. IEEE, 1977, pp. 36–57.

[21] R. W. Erickson, “Large signals in switching converters,” Ph.D. dissertation, California Institute of Technology, 1983.

[22] R. W. Erickson, S. Ćuk, and R. D. Middlebrook, “Large-signal modeling and analysis of switching regulators,” in *IEEE power electronics specialists conference records*, 1982, pp. 240–250.

[23] A. Massarini, U. Reggiani, and M. K. Kazimierczuk, “Analysis of networks with ideal switches by state equations,” *Circuits and Systems I: Fundamental Theory and Applications, IEEE Transactions on*, vol. 44, no. 8, pp. 692–697, 1997.

[24] J. Sun and H. Grotstollen, “Symbolic analysis methods for averaged modeling of switching power converters,” *Power Electronics, IEEE Transactions on*, vol. 12, no. 3, pp. 537–546, 1997.

[25] M. L. Heldwein, “EMC filtering of three-phase PWM converters,” Ph.D. dissertation, Diss., Eidgenössische Technische Hochschule ETH Zürich, Nr. 17554, 2008, 2008.

[26] M. L. Heldwein, T. Nussbaumer, and J. W. Kolar, “Differential mode EMC input filter design for three-phase AC-DC-AC sparse matrix PWM converters,” in *IEEE 35th Annual Power Electronics Specialists Conference, 2004. PESC’04.*, vol. 1. IEEE, 2004, pp. 284–291.

[27] K. Mainali and R. Oruganti, “Conducted emi mitigation techniques for switch-mode power converters: A survey,” *Power Electronics, IEEE Transactions on*, vol. 25, no. 9, pp. 2344–2356, 2010.

[28] P. Pejović, “Simulation of power electronic converters using quasi steady state approximation,” *Electronics*, vol. 16, no. 2, pp. 153–158, 2012.

[29] S. Buso and P. Mattavelli, “Digital control in power electronics,” *Lectures on Power Electronics*, vol. 1, no. 1, pp. 1–158, 2006.

[30] J. C. Butcher, *Numerical Methods for Ordinary Differential Equations*. John Wiley & Sons, Inc., 2008.

[31] A. M. Luciano and A. G. Strollo, “A fast time-domain algorithm for the simulation of switching power converters,” *Power Electronics, IEEE Transactions on*, vol. 5, no. 3, pp. 363–370, 1990.

[32] R. W. Erickson and D. Maksimovic, *Fundamentals of power electronics*. Springer Science & Business Media, 2007.

[33] M. Glišić and P. Pejović, “Stability issues in peak limiting current mode controlled buck converter,” in *17th International Symposium on Power Electronics — Ee 2013*, Novi Sad, Oct. 30/Nov. 01, 2013.

[34] P. Pejović and M. Glišić, “Conduction modes of a peak limiting current mode controlled buck converter,” in *X International Symposium on Industrial Electronics INDEL*, Banja Luka, Nov. 06–08, 2014, pp. 67–72.

[35] Maxima, a Computer Algebra System. [Online]. Available: http://maxima.sourceforge.net/

[36] Python. [Online]. Available: https://www.python.org/

[37] T. E. Oliphant, “Python for scientific computing,” *Computing in Science & Engineering*, vol. 9, no. 3, pp. 10–20, 2007.

[38] NumPy. [Online]. Available: http://www.numpy.org/

[39] SciPy. [Online]. Available: http://www.scipy.org/

[40] matplotlib. [Online]. Available: http://matplotlib.org/

[41] Julia. [Online]. Available: http://julialang.org/

[42] J. Bezanson, A. Edelman, S. Karpinski, and V. B. Shah, “Julia: A fresh approach to numerical computing,” *arXiv preprint arXiv:1411.1607*, 2014.